NTIS $8.00

UAH-MSFC/NASA Cooperative Agreement

Modification No. 1

DRA

Project III

"ANALYSIS OF THERMAL ENVIRONMENT IN THE THRUSTOR CAVITY OF SPACE VEHICLES"

INTERIM REPORT

by

J. N. Chiou

and

J. J. Brainerd

Department of Fluid & Thermal Engineering
School of Graduate Studies and Research
The University of Alabama in Huntsville
P. O. Box 1247
Huntsville, Alabama 35807

October 1972

38

Foreword

The work described in this report is part of a continuing effort being carried out at UAH. The participants in this study have maintained a close liaison with Mr. Bob Fisher and Mr. Jerry Vanneman of NASA-MSFC,
The purpose of this close liaison has been to discuss problems, results, and new techniques in order that the results of this study be as beneficial to this group as possible. Consequently, many informal recommendations have been made, which may or may not be formalized when this work is completed.

INTRODUCTION

The Problem

The problem to be studied stems from the requirement for the control system thrustors of a space shuttle type vehicle, necessary for exo-atmospheric flight control, to be buried within the heat shield of the vehicle so that interference heating will be reduced during flight in the atmosphere. The geometry of a typical installation is illustrated in Figure 1. During atmospheric flight, the non-firing thrustor nozzle represents a cavity in the surface of the vehicle. The interaction of the hypersonic external flow with the cavity produces excess local heating which must be ameliorated.

Mechanical systems, such as a cover that slides over the nozzle exit, and active cooling systems introduce other problems besides adding undesirable weight and complexity to the vehicle. The simple expedient of increasing heat shield thickness in the region of the cavity would ultimately imply additional ablation in the area and probable change in nozzle size or shape from flight to flight. This may require additional refurbishment before each flight.

This study, therefore, is aimed at determining the mechanisms involved in producing the high local heating rates in and around the thrustor nozzle in non-firing condition. In such a case, the nozzle is treated simply as a cavity.

Literature Survey

A survey of the literature available on this and related problems revealed that very few results applicable to this particular problem have appeared in the open literature. Of the papers reviewed, only those referenced in this report appear to have direct consequence for this study. A more complete bibliography on cavity flows will be included in the final report for this study.

Experimental Program

A test program, conducted at AEDC by personnel of General Dynamics Corp., has produced some results directly applicable to this study. In order to provide a basis for comparison or for development of empirical relations, a short study was made to compare the flow conditions in the wind-tunnel studies with flight conditions. Of particular concern was the question of whether the boundary layer ahead of the cavity was laminar or turbulent in either the wind tunnel or flight regimes. A map of these conditions is shown in Figures 2 and 3. The wind tunnel conditions are for the von Karman Facility, Tunnel B, at AEDC[1]. The flight conditions are for a typical reentry corridor,[2] with no special attempt to relate the reentry trajectory to the space shuttle vehicle.

In all of the wind tunnel tests and in the flight regime, it is expected that the boundary layer ahead of the nozzle cavity will be fully developed and turbulent. In flight, but not in the wind tunnel, the boundary layer probably should contain significant amounts of ablation products at the nozzle location. No attempt is made to account for the influence of ablation or surface heating ahead of the nozzle area, except to account for the total temperature profile through the boundary layer and, hence, the total pressure profile.

Since the analysis of the experimental data is being carried out at General Dynamics, no general discussion of the results will be made here. In so far as possible, comparisons of the results of this study are made with the raw data of the experiments.[3] These confirm the qualitative features of the flow derived from theoretical analysis.

ANALYSIS

Fundamental Features of the Flow

In the flight vehicle, the thrustor nozzles are to be installed in curved surfaces. Presumably, the local radius of curvature of the body will be sufficiently large cf. the nozzle diameter so that the effects of surface curvature will be at most of secondary importance in this problem. The wind tunnel test program centered mainly on axially-symmetric nozzles set into a flat-plate model. In this study, only one basic configuration is considered. This is the axially-symmetric nozzle cavity set into a flat plate with the nozzle axis normal to the plate surface, as in Fig. 1. The flow would be two-dimensional in the absence of the cavity. The disturbance produced by the cavity is three-dimensional, which greatly adds to the complexity of the problem.

Sketches of a two-dimensional cavity flow and the central plane of the present problem are shown in Fig. 4. In the two-dimensional problem, the boundary layer separates from the upstream edge of the cavity. The dividing streamline leaves the separation point and intersects the downstream surface of the cavity, at a stagnation point. The location of the stagnation point depends upon several parameters such as cavity height and cavity width. But, in the steady state 2-D solution, the stagnation streamline is the separation streamline. The flow within the cavity circulates about a vortex core, driven by the shearing stress along the dividing streamline.

In the 3-D case, fluid may move in the y direction so that mass may be injected into the cavity in the central plane. In a steady state, the mass flowing into the cavity near the center line must flow out of the cavity at some distance from the central plane. The three dimensionality of the cavity clearly shows that stagnation should occur only in the central plane, so that the lateral flow would be expected to occur. The injected mass flow would increase the angular momentum of the flow in the cavity, thereby strengthening the vortex within the cavity. This vortex must exit the cavity with the outflow and be washed downstream. The

resultant vortex shape is reminiscent of the classical horseshoe vortex of a lifting wing of finite span. (Fig. 5) A crude model has been devised to indicate the influence of this vortex on the pressure distribution in the neighborhood of the cavity. The model is discussed in some detail in the next section of this report including a comparison with experimental results. No attempt has been made to include compressibility effects, the influence of the boundary layer ahead of the cavity, or the interaction of the trailing vortex with the boundary layer downstream of the cavity.

The strength of the vortex within the cavity is difficult to ascertain. Values may be inferred from two-dimensional results, but great care must be exercised in order to avoid erroneous conclusions. A discussion of two-dimensional and axially symmetric (annular cavity) studies is presented in a succeeding section of this report. As a result of these studies, some tentative conclusions may be drawn, particularly in reference to future experimentation.

Horseshoe Vortex Model

The vortex within the cavity in the three-dimensional case must extend "to infinity," close on itself, or end on a solid wall, according to a theorem due to Helmholtz. It has also been shown that in viscous flow, a vortex line may end on a solid boundary only at a stagnation point. Consequently, the vortex generated in the cavity in the case under consideration must have the form as described earlier (Fig. 5).

The horseshoe vortex must be one of the dominant features of the cavity-boundary layer interaction. The flow induced by the vortex would modify pressure distributions and velocity fields to a significant degree. Viscosity and compressibility would modify these effects, of course.

A crude initial model was devised by considering the superposition of a uniform flow on the flow due to a horseshoe vortex in steady, potential flow. Viscosity, compressibility and body forces are neglected. The boundary condition that there be no flow through the surface is imposed by the method of images. The cavity was not included in the geometry.

The velocity field induced by a horseshoe vortex lying in an xy plane at a height z_1 above the surface is given by [4]:

$$\vec{V}_1 = \frac{\Gamma}{4\pi}\left[\frac{(z-z_1)\vec{i} + (x-x_1)\vec{k}}{(z-z_1)^2 + (x_1-x)^2}\left\{\frac{y-y_1}{\sqrt{(x-x_1)^2+(y-y_1)^2+(z-z_1)^2}}\right.\right.$$

$$\left. - \frac{y-y_2}{\sqrt{(x-x_1)^2+(y-y_2)^2+(z-z_1)^2}}\right\}$$

$$+ \frac{(z-z_1)\vec{j} + (y_1-y)\vec{k}}{(z-z_1)^2 + (y_1-y)^2}\left\{1 + \frac{x-x_1}{\sqrt{(x-x_1)^2+(y-y_1)^2+(z-z_1)^2}}\right\}$$

$$\left. - \frac{(z-z_1)\vec{j} + (y_2-y)\vec{k}}{(z-z_1)^2 + (y_2-y)^2}\left\{1 + \frac{x-x_1}{\sqrt{(x-x_1)^2+(y-y_2)^2+(z-z_1)^2}}\right\}\right]$$

where Γ is the circulation. The model is illustrated in Fig. 6. In comparison of this initial model with the actual flow geometry, the length of segment A-B of the horseshoe vortex is taken as being equal to the nozzle exit diameter.

Since the image system utilized above guarantees that there be no flow through the surface $z = 0$, this model shows no flow into the cavity. In order to obtain a downwash velocity over the cavity opening, an additional line vortex segment is superimposed, on the flow field in the upper half plane. This new vortex segment is parallel to the segment AB, at a distance equal to z, below the cavity surface. Thus the velocity vector is obtained:

$$\vec{V} = U_\infty \vec{i} + \frac{\Gamma}{4\pi}\left[\frac{(z-z_1)\vec{i} + (x_1-x)\vec{k}}{(z-z_1)^2 + (x_1-x)^2}\left\{\frac{y-y_1}{\sqrt{(x-x_1)^2+(y-y_1)^2+(z-z_1)^2}} - \frac{y-y_2}{\sqrt{(x-x_1)^2+(y-y_2)^2+(z-z_1)^2}}\right\}\right.$$

$$- \frac{(z+z_1)\vec{i} + (x_1-x)\vec{k}}{(z+z_1)^2 + (x_1-x)^2}\left\{\frac{y-y_1}{\sqrt{(x-x_1)^2+(y-y_1)^2+(z-z_1)^2}} - \frac{y-y_2}{\sqrt{(x-x_1)^2+(y-y_2)^2+(z-z_1)^2}}\right\}$$

$$+ \frac{(z-z_1)\vec{j} + (y_1-y)\vec{k}}{(z-z_1)^2 + (y_1-y)^2}\left\{1 + \frac{x-x_1}{\sqrt{(x-x_1)^2+(y-y_1)^2+(z-z_1)^2}}\right\}$$

$$- \frac{(z+z_1)\vec{j} + (y_1-y)\vec{k}}{(z+z_1)^2 + (y_1-y)^2}\left\{1 + \frac{x-x_1}{\sqrt{(x-x_1)^2+(y-y_1)^2+(z+z_1)^2}}\right\}$$

$$- \frac{(z-z_1)\vec{j} + (y_2-y)\vec{k}}{(z-z_1)^2 + (y_2-y)^2}\left\{1 + \frac{x-x_1}{\sqrt{(x-x_1)^2+(y-y_2)^2+(z-z_1)^2}}\right\}$$

$$\left. + \frac{(z+z_1)\vec{j} + (y_2-y)\vec{k}}{(z+z_1)^2 + (y_2-y)^2}\left\{1 + \frac{x-x_1}{\sqrt{(x-x_1)^2+(y-y_2)^2+(z+z_1)^2}}\right\}\right]$$

In this model the compressibility, the boundary conditions on the cavity walls, and the boundary layer upstream of the cavity have not been taken into account. The pressure at any point is obtained from the incompressible Bernoulli Equation.

Vortex Strength

Since the velocity and pressure fields in the vortex model are dependent upon the strength of the vortex, Γ, (circulation) some method for predicting the value of Γ must be specified. In the absence of any theoretical study which would specify Γ for the geometry of this problem, an appeal is made to the qualitative similarity between the flow in the plane of symmetry and the flow in a two-dimensional problem.

Burggraf[5] has given the following relation for the vorticity, ω, in a two-dimensional rectangular cavity:

$$\omega = \frac{U_\infty}{a}\left[\frac{0.0615}{(1+b/a)}\,\frac{(a/L)^{2/3}}{\overline{F^2}}\right]^{1/2}$$

where a is the width of the cavity, b is the depth of the cavity, L is the "effective running length" to the separation point (in our case, the distance from the leading edge of the plate to the edge of the cavity), and $\overline{F^2}$ is the root-mean-square of the surface velocity over the perimeter of the cavity.

The values of $\overline{F^2}$ given by Burggraf are:

b/a	1/4	1/3	1/2	1	2	3	4
$\overline{F^2}$	.01092	.01732	.03122	.07029	.12488	.15583	.17466

For constant values of U_∞, L, and b, the variation of the vorticity ω with cavity width, a, may be obtained from

$$\frac{\omega}{\omega_1} = \left(\frac{a_1}{a}\right)\left[\frac{(1+b/a_1)\,\overline{F_1^2}}{(1+b/a)\,\overline{F^2}}\right]^{1/2}$$

where the subscript 1 denotes a reference condition. With a_{ref} taken as being equal to b, this variation of ω with a is shown in Fig. 8.

The heat transfer rate on the reattachment (downstream) wall of the cavity is given by Hodgson[6] as:

$$\frac{q}{q_1} = \left(\frac{a}{a_1}\right)^{3/4}$$

This variation is also shown in Fig. 8.

Burggraf's theory is based upon the plane, inviscid, incompressible, but rotational, flow over a rectangular cavity. According to his theory, the heat transfer rate depends only on the cavity width-to-depth ratio. Hodgson includes compressibility. His results indicate that the heat transfer rate may vary with cavity width, even with b/a fixed, thus revealing a scaling effect.

A comparison of the heat transfer rates on the reattachment wall predicted by these two-dimensional theories with the rates obtained in the plane of symmetry in the three-dimensional tests in a wind tunnel are shown in Fig. 9. Two items are immediately indicated by this comparison: 1) the test data is much steeper in the reattachment zone than that predicted by either Burggraf's or Hodgson's theory; and 2) the tests show a decrease in reattachment heating with decreasing nozzle diameter as evidenced by tests with a two inch diameter nozzle, and tests with a one inch diameter nozzle. Hence, scaling may be a very important factor in the application of the wind tunnel test results to the flight vehicle.

The vorticity predicted by Burggraf's two-dimensional theory was taken to predict the circulation Γ of the horseshoe vortex in the three-dimensional model discussed earlier. The pressure distribution obtained from this model are shown in Fig. 10. Experimental results, shown in Figs. 11 - 21, show qualitative agreement.

Experimental Results

Tests of the axially symmetric nozzle cavity in a flat plate at various angles of attack, were conducted in the AEDC-VKF Tunnel B, for various Reynolds Numbers and at a nominal Mach Number of 8. Wind tunnel operating conditions for the

various tests are listed in Table I. The flow conditions on the flat plate for the six cases shown in this report are listed in Table II. Isobars and isotherms in the vicinity of the cavity for these six cases are shown in Figs. 11 - 21.

The major qualitative features of the pressure field in these tests are predicted by the horseshoe vortex model of the flow. Of particular interest in this respect is the high pressure zones just outside the cavity at $\theta = 90^{\circ}$, 270°, as predicted. The major discrepancy in trends between the experimental results and the horseshoe vortex model occurs just downstream of the cavity on the plane of symmetry, $\theta = 0^{\circ}$. Where the theory shows a decreasing pressure, the experiment shows a low pressure on the cavity lip and a rising pressure downstream. This discrepancy could be due to separation as the reattached flow tries to negotiate the sharp lip of the cavity exit. In any event, the agreement is remarkable in view of the crudeness of the theoretical model. This clearly demonstrates that the horseshoe vortex is the key feature of the flow field.

One aspect of the test results is very interesting. In an effort to reduce the peak heating rate in the cavity, which occurs at the reattachment point, cold gas was bled (i.e., at low thrustor chamber pressure) through the nozzle in cases 2 and 3. With increasing bleed rate the stagnation point (reattachment point) moved farther into the cavity and the reattachment wall temperature increased. Thus the nozzle bleed aggravated the heating problem instead of ameliorating it. The horseshoe vortex model of the flow explains this phenomenon. Since for the bleed cases (as opposed to thrustor firing) the stagnation pressure of the bleed gas is much much less than the stagnation pressure of the external flow. As indicated in Fig. 22, the recirculating gas is not much influenced by the bleed gas which must separate from the downstream (reattachment) wall just above the nozzle throat. Consequently, all of the bleed gas must be directed upward along the upstream wall. This injection of the bleed gas increases the angular momentum of the cavity flow, and therefore increases the vortex strength. The stronger vortex, in turn pulls in more of the external flow, again increasing the angular momentum in the cavity. The new stagnation streamline, moreover, originates higher in the upstream boundary layer so that it has a higher stagnation temperature than the streamlines closer to the wall, due to heat transfer to the plate.

Cavity Shape

Thomke[7] has studied the flow of turbulent boundary layers flowing over axially-symmetric cavities (annular grooves cut into the surface of a right-circular cone). The experimental tests were conducted at Mach Numbers of 2.0, 2.5, 3.0, and 4.0 and wind tunnel unit Reynold's Numbers of 0.95, 1.02, 1.36, 1.43, and 1.30 million. A comparison of pressure distributions taken at $M = 2.0$, $R_e = 0.95 \times 10^6$ per inch for two cavity shapes is shown in Fig. 23.

The test results clearly show that rounding the reattachment wall produces a much flatter (almost constant) pressure distribution along the cavity floor. Additionally, the rounded corner results in a lower peak pressure, and the point of maximum pressure being moved downstream. These results would imply that rounding the corner would reduce heating in or near the cavity.

RESULTS

At this stage of the study, conclusions may be drawn:

1. The boundary layer-cavity interaction generates a horseshoe vortex reminiscent of the vortex system of a wing of finite span.
2. The pressure distribution in and around the cavity is influenced very strongly by this horseshoe vortex. The influence of this vortex will extend far downstream, and laterally beyond the sides of the cavity.
3. Bleeding cold gas through the nozzle increases the strength of the vortex and, consequently, increases the peak heating rate in the nozzle.
4. Variation of cavity geometry could tend to weaken the vortex, thereby relieving the heating problem.
5. The key to passive system heat protection in the region of the cavity is the control of the vortex strength by shaping of the nozzle.

Work is continuing to develop a means for predicting the vortex strength and thereby be able to calculate heating rates for the cavity flow. These means will have a theoretical base, but will rely heavily on experimental data. Continuation of this work could lead to procedures for optimizing nozzle shapes in order to find the optimal shape when thrustor performance and cavity heating are both considered. Continued support of the UAH effort is necessary in order to be able to develop sufficiently accurate techniques for prediction purposes.

REFERENCES

1. -- Test Facilities Handbook (Ninth Edition), Arnold Engineering Development Center, Tennessee (July 1971).

2. Hermann, R.: Hypersonic Aerodynamic Problems at Re-entry of Space Vehicles, UARI Res. Rept. No. 29, University of Alabama Research Institute, Huntsville, Alabama (November 1965).

3. -- Space Shuttle Attitude Control System (ACS) Thrustor Penetration Heating, Second Quarterly Progress Report, Contract NAS8-27683, for NASA-MSFC; Report No. 632-TP-3, General Dynamics/Convair Aerospace Division, San Diego (January 1972).

4. Robinson, A. and Laurmann, J. A.: Wing Theory, Cambridge Univ. Press (1953).

5. Burggraf, O. R.: "A Model of Steady Separated Flow in Rectangular Cavities at High Reynold's Number", Proc. 1965 Heat Transf. and Fluid Mech. Inst., (A. F. Charwat, ed.) Stanford Univ. Press, pp 190-229 (1965).

6. Hodgson, J. W.: "Heat Transfer in Separated Laminar Hypersonic Flow", AIAA Jour., Vol. 8, No. 12, pp 2291-2293 (December 1970).

7. Thomke, G. J.: Separation and Reattachment of Supersonic Turbulent Layer Behind Downstream Facing Steps and Over Cavities, Report No. SM-43602, STAR Accession No. N64-22007, Douglas Airc., Santa Monica, Calif. (1964).

Table I. Wind Tunnel Operating Conditions From AEDC VKF Tunnel B

Mach No.	Stagnation Pressure N/m^2 (lb_f/in^2)	Stagnation Temp. ^oK (^oR)	Static Temp. ^oK (^oR)	Static Press. N/m^2 (lb_f/in^2)	Freestream Density kg/m^3 ($slug/ft^3$)	Reynolds No. $10^6/m$ ($10^6/ft$)	Freestream Velocity m/sec (ft/sec)
7.895	8.963×10^5 (130)	672.2 (1210)	50.0 (90)	96.53 (.014)	$.224 \times 10^{-3}$ (1.399×10^{-5})	2.296 (.7)	1117 (3665)
7.968	28.958×10^5 (420)	716.7 (1290)	52.2 (94)	303.37 (.044)	$.647 \times 10^{-3}$ (4.04×10^{-5})	6.562 (2.0)	1152 (3780)
8.013	59.639×10^5 (865)	746.7 (1344)	53.9 (97)	599.84 (.087)	1.219×10^{-3} (7.615×10^{-5})	12.139 (3.7)	1180 (3870)

Table II. Flat Plate Flow Field Conditions in AEDC Test

Case No.	M_∞	T_∞ °R	P_∞ lb_f/in^2	U_∞ ft/sec	P_{oj} lb_f/in^2	T_{oj} °R	θ deg.	D_j in.
1	8.00	97.6	.089	3874	0	527	0.13	2
2	8.00	98.3	.089	3887	6.9	530	0.13	2
3	8.00	98.3	.089	3887	25.9	530	0.13	2
4	8.00	98.3	.089	3877	0	571	-0.08	1
5	8.00	97.8	.089	3877	0	573	-0.03	1/2
6	7.92	84.0	.014	3557	0	561	-0.08	2

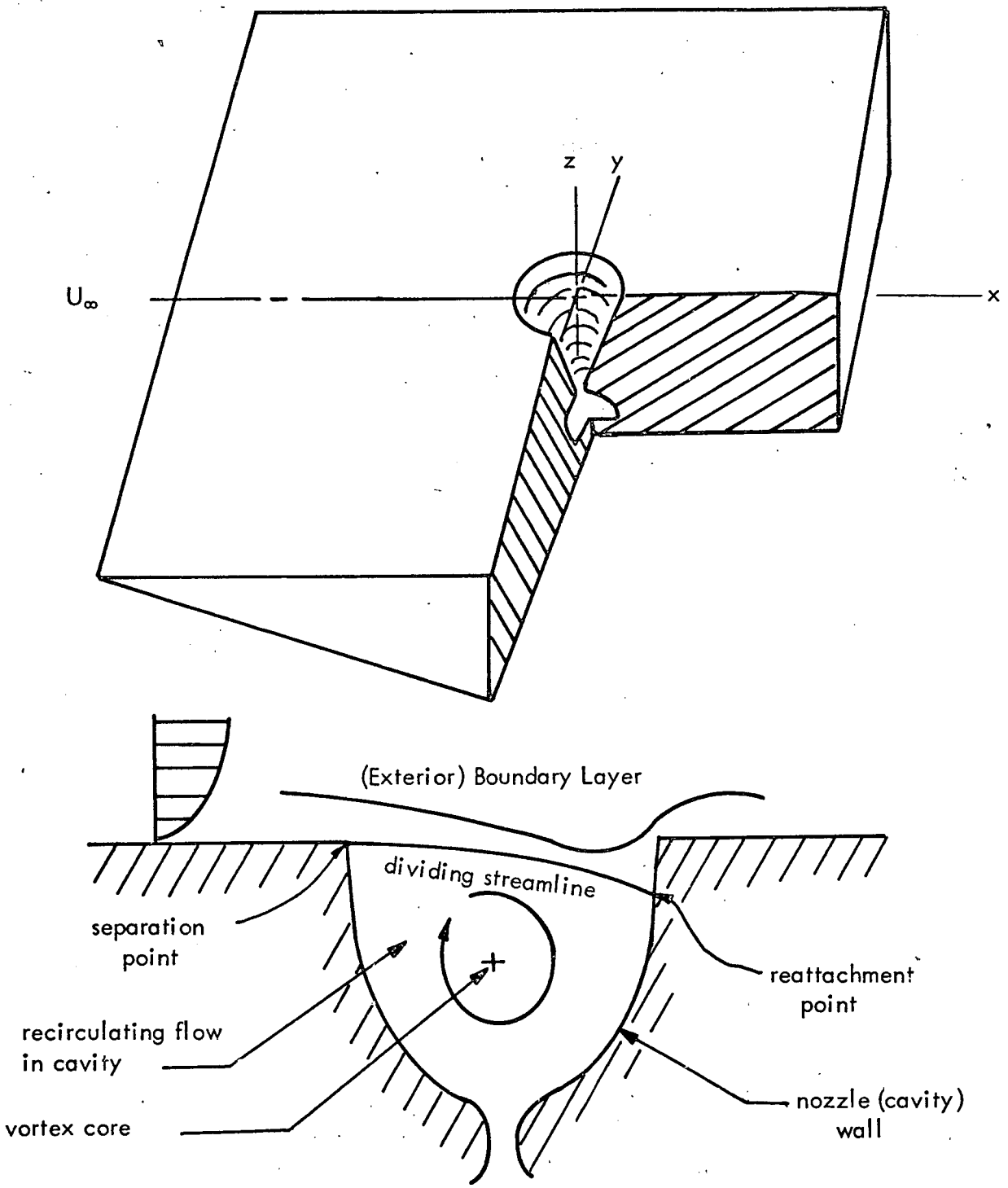

FIG. 1. Typical Installation of an Axially Symmetric Nozzle in a Flat Plate.

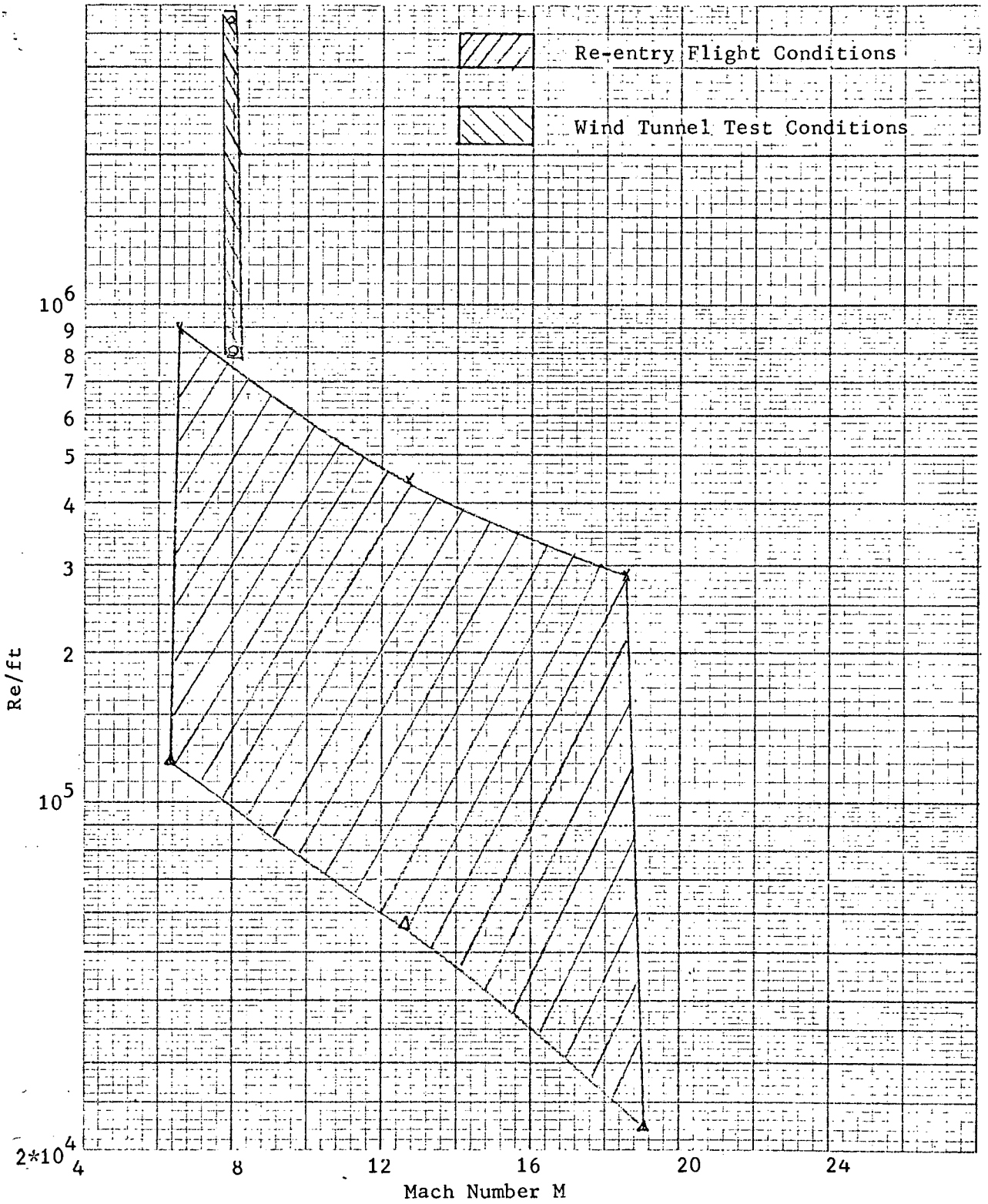

Fig. 2. Comparison of Mach Numbers between Re-entry Flight and Wind Tunnel Test Conditions

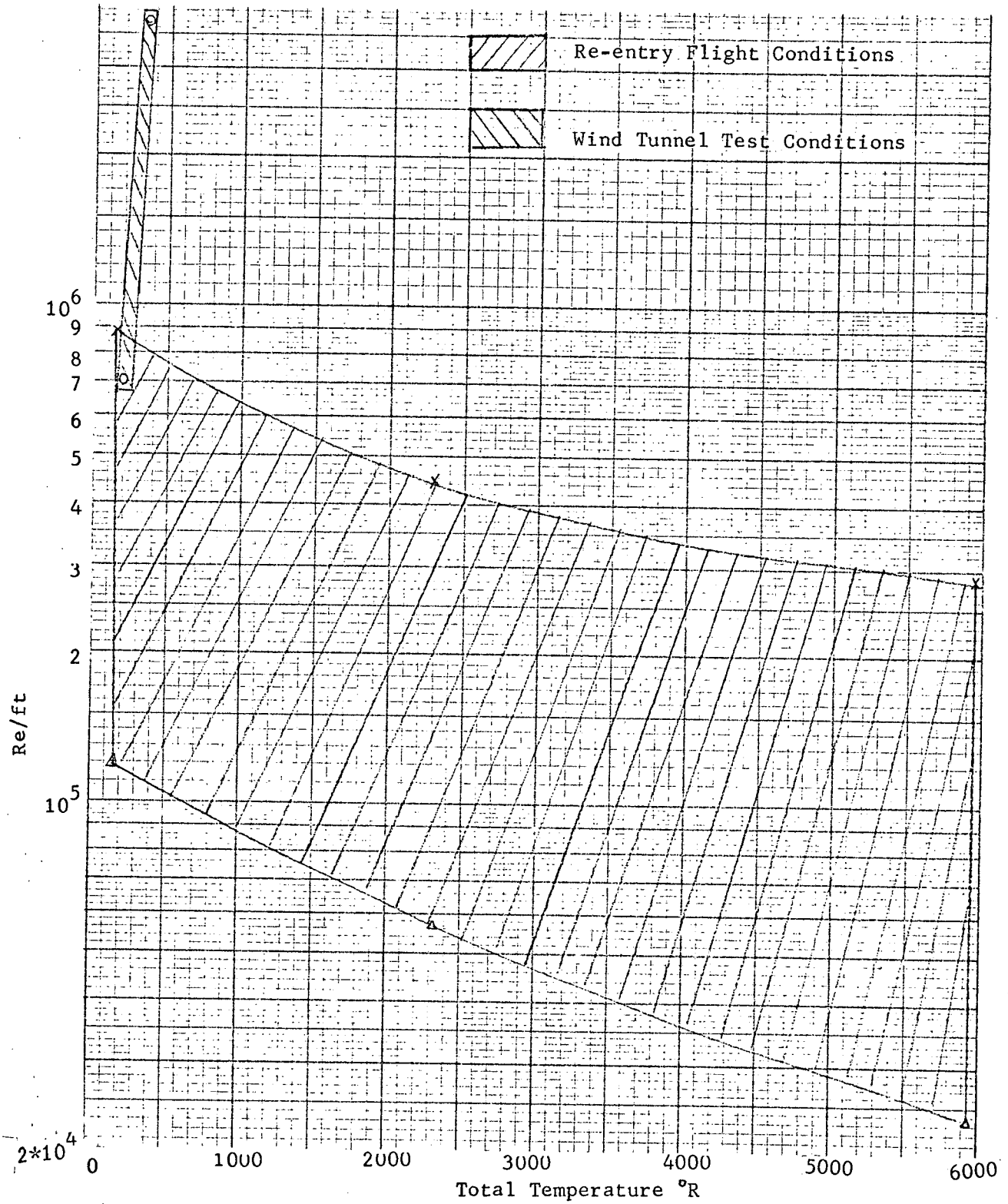

Fig. 3. Comparison of Total Temperature between Re-entry Flight and Wind Tunnel Test Conditions

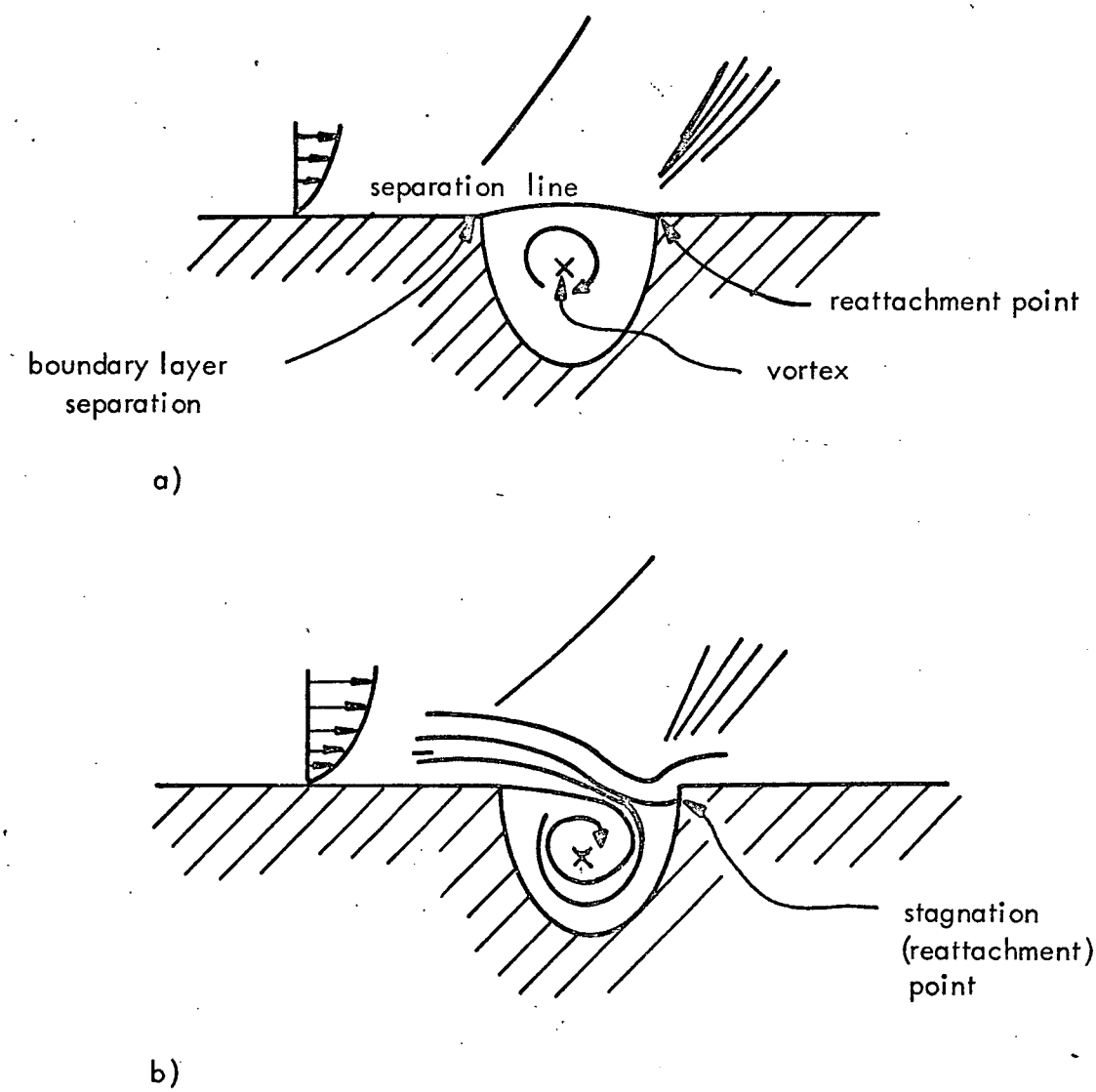

FIG. 4. Sketches of Flow in Cavity.

a) Two-dimensional Flow

b) Plane of Symmetry in 3-D Case

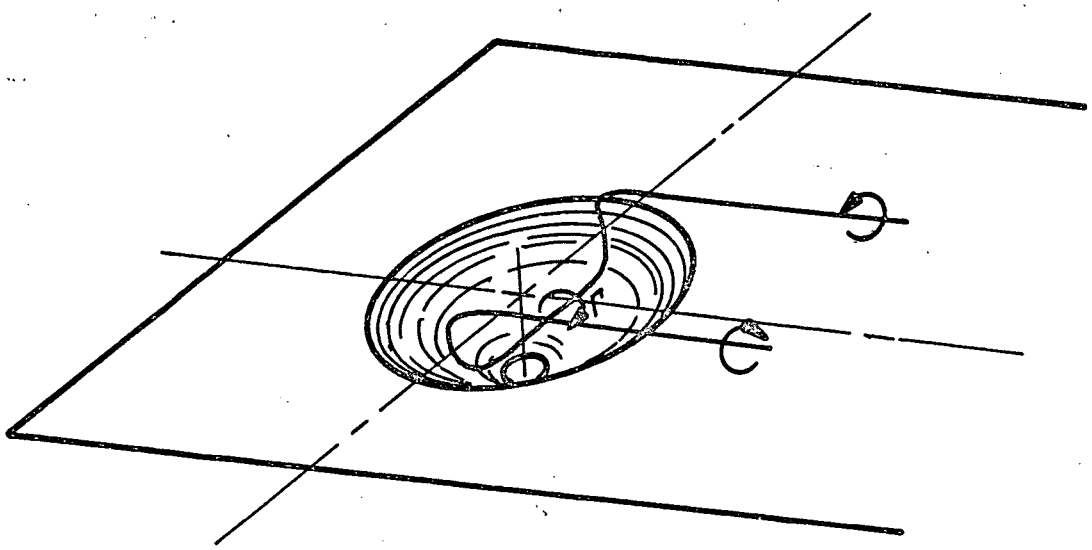

FIG. 5. Horseshoe Vortex for Three-Dimensional Cavity Flow.

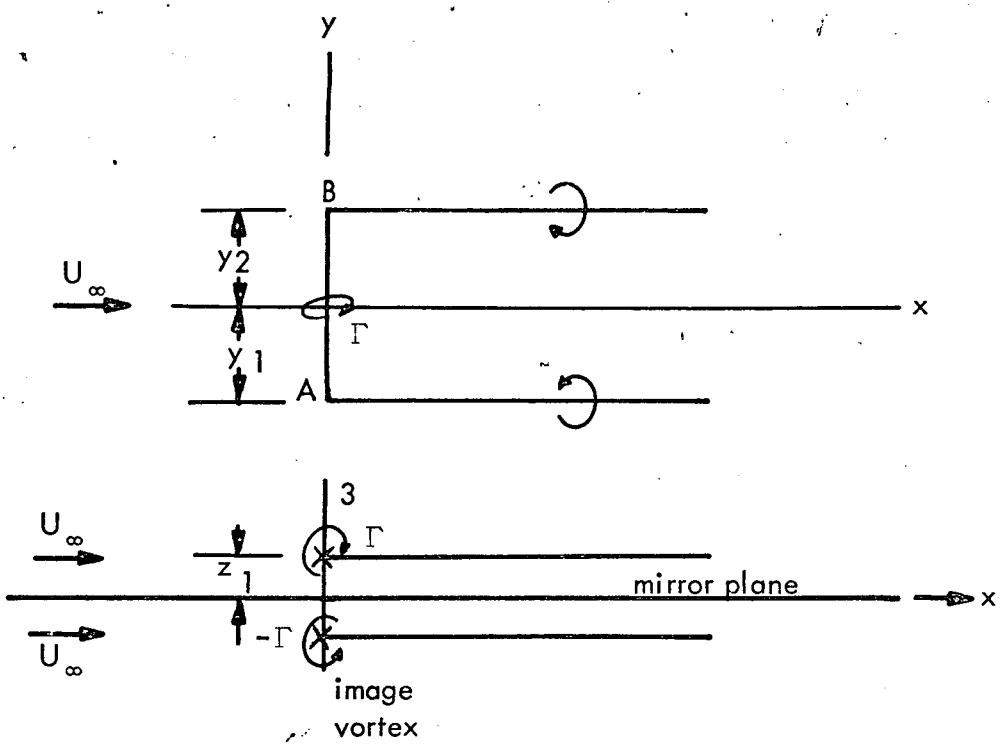

FIG. 6. Superposition of Horseshoe Vortex and Free Stream, Using Method of Images to Enforce no Flow Through the Surface.

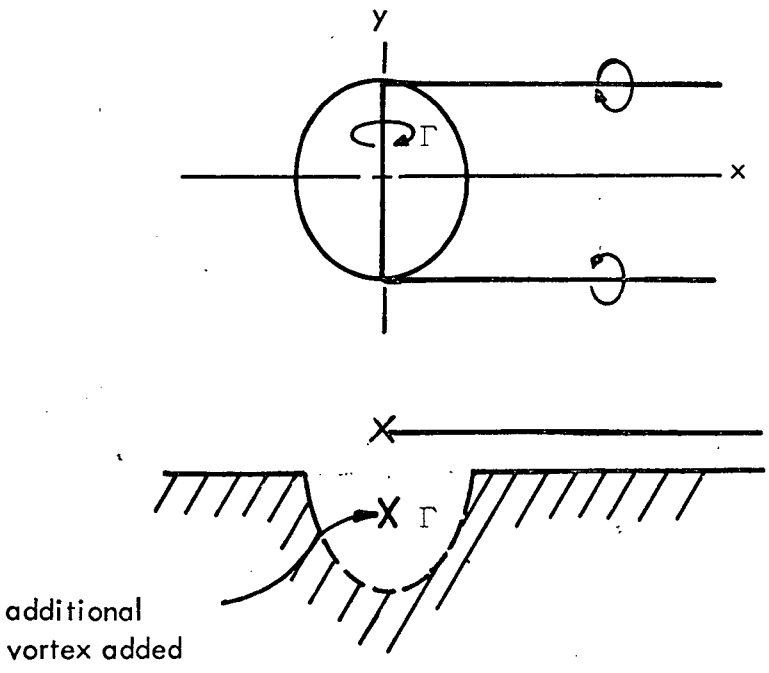

FIG. 7. Horseshoe Vortex Model With Additional Vortex Segment to Induce Flow Through Cavity Exit Plane.

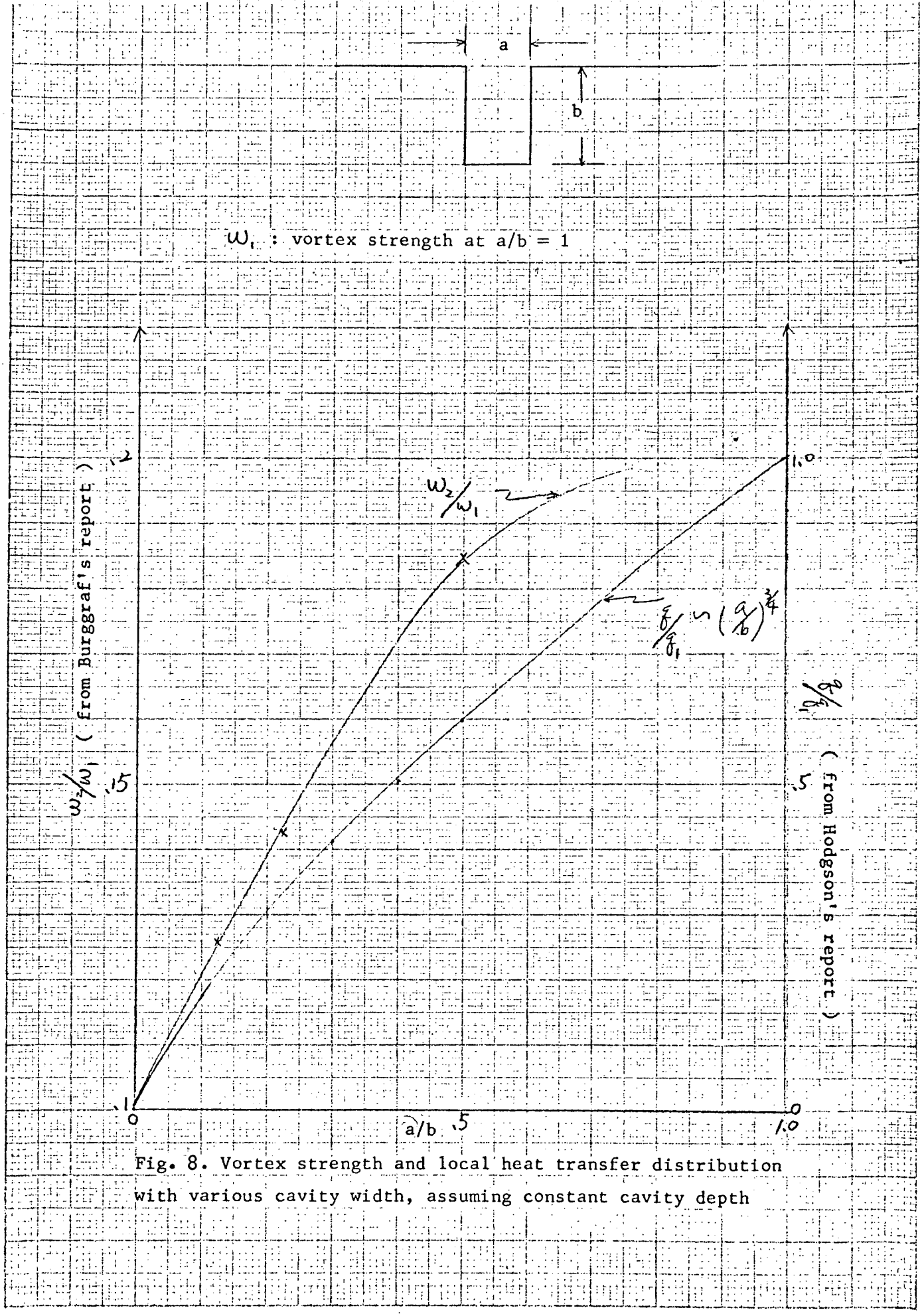

Fig. 8. Vortex strength and local heat transfer distribution with various cavity width, assuming constant cavity depth

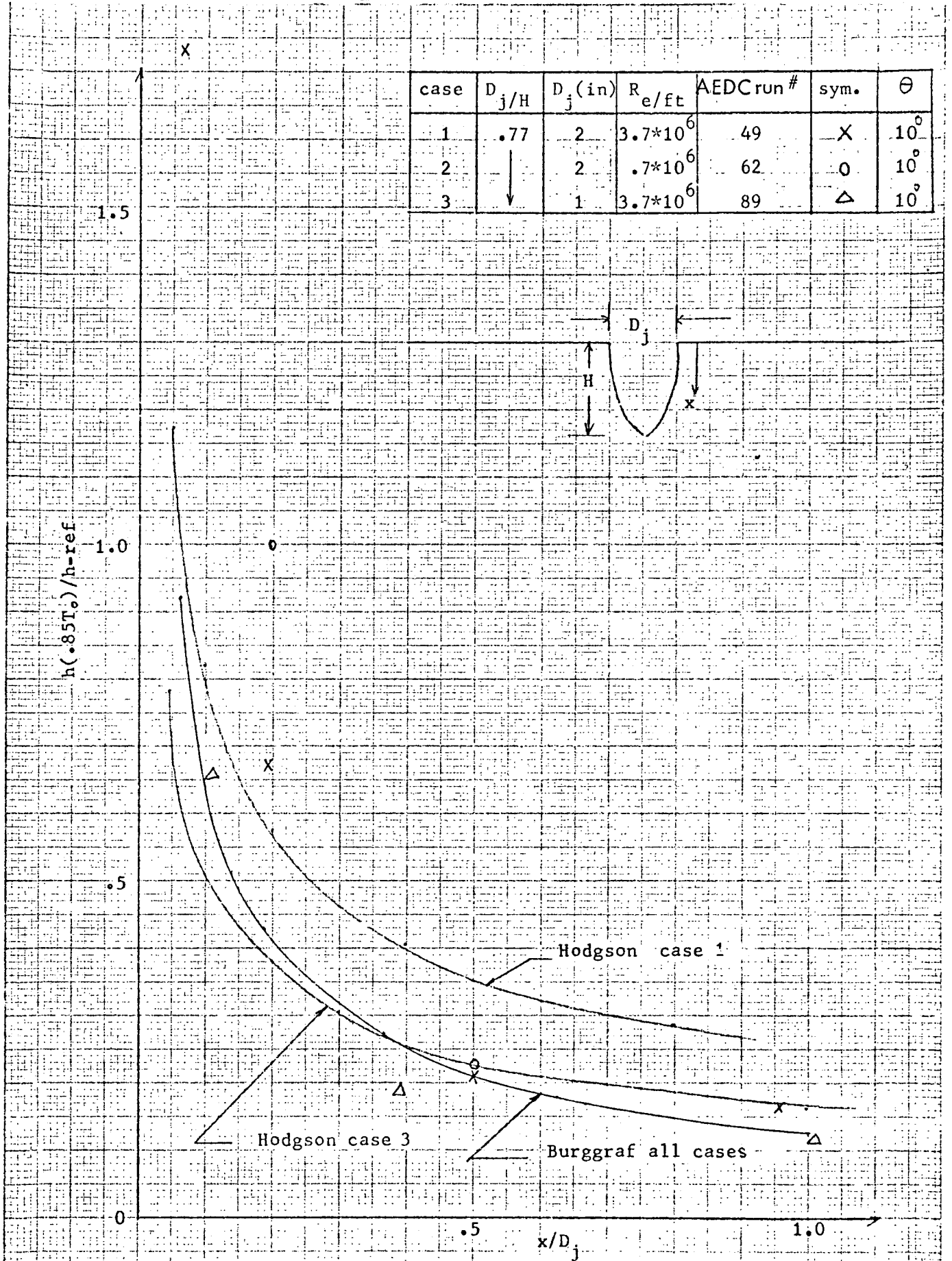

case	$D_{j/H}$	D_j (in)	$R_{e/ft}$	AEDC run #	sym.	θ
1	.77	2	$3.7*10^6$	49	X	10^0
2	↓	2	$.7*10^6$	62	0	10^0
3		1	$3.7*10^6$	89	△	10^0

Fig. 9 COMPARISON BETWEEN CENTRAL PLANE REATTACHMENT WALL AND TWO DIMENSIONAL THEORIES, WHERE ANGLE OF ATTACK IS 0

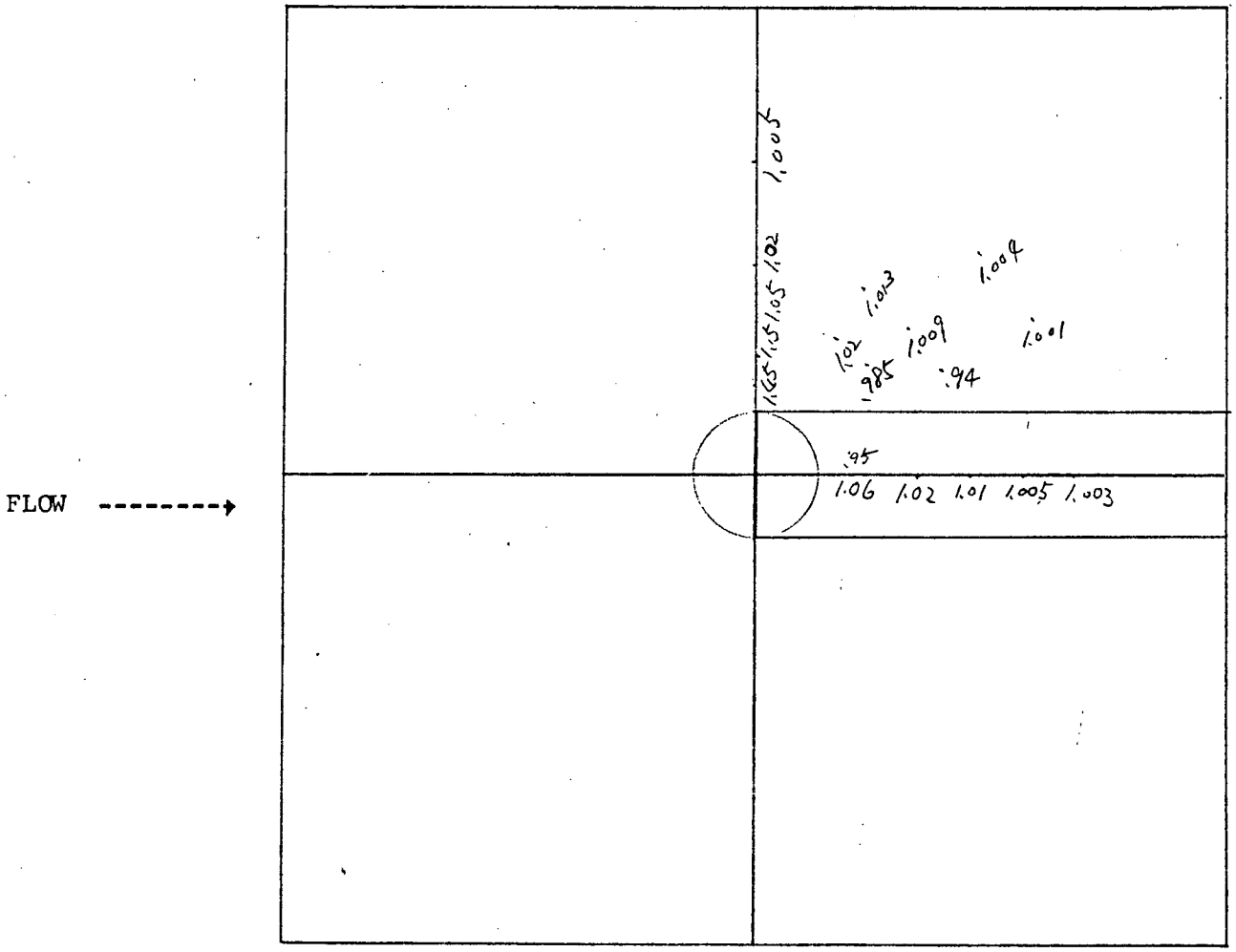

Fig. 10. PRIDICTED PRESSURE DISTRIBUTION BY HYDRODYNAMIC STUDY UNDER CASE 1

FLOW ---------▶

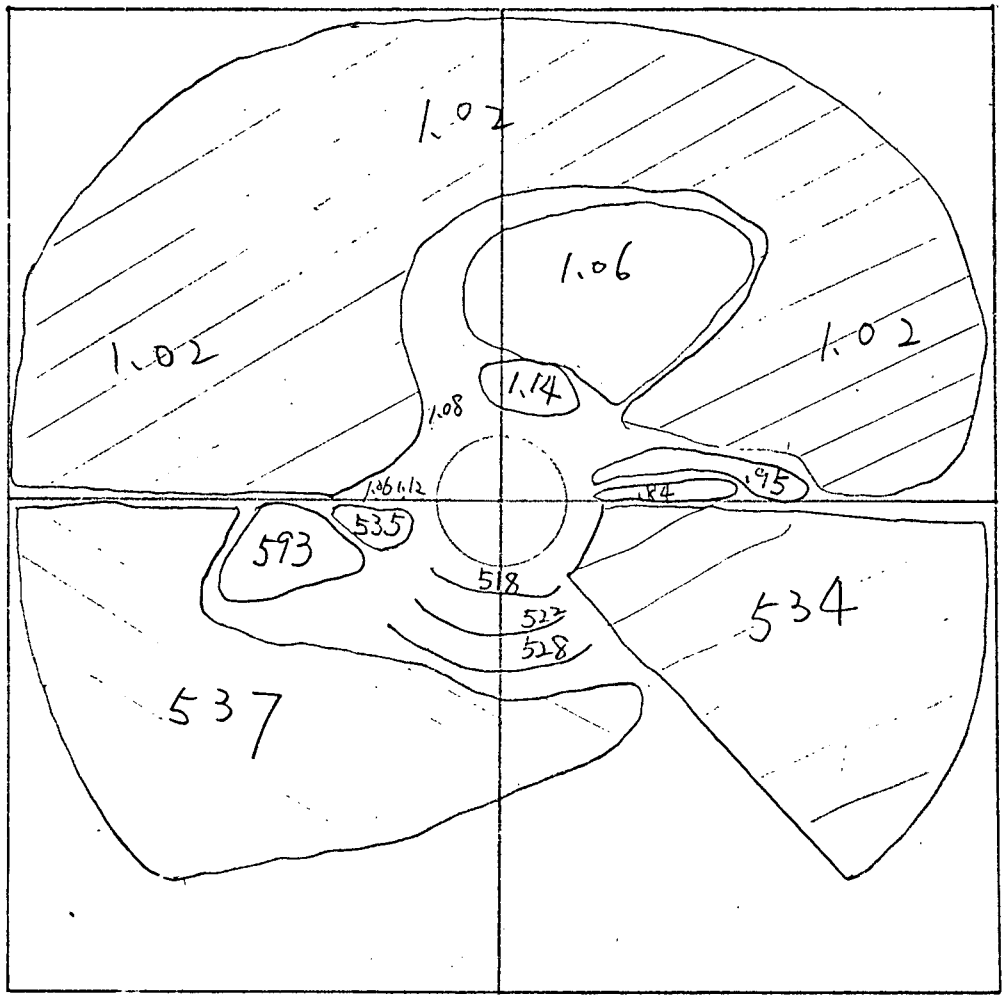

Fig. 11. ISOBAR (upper half, normalized by P-inf) AND ISOTHERM °R (lower half) UNDER CASE 1

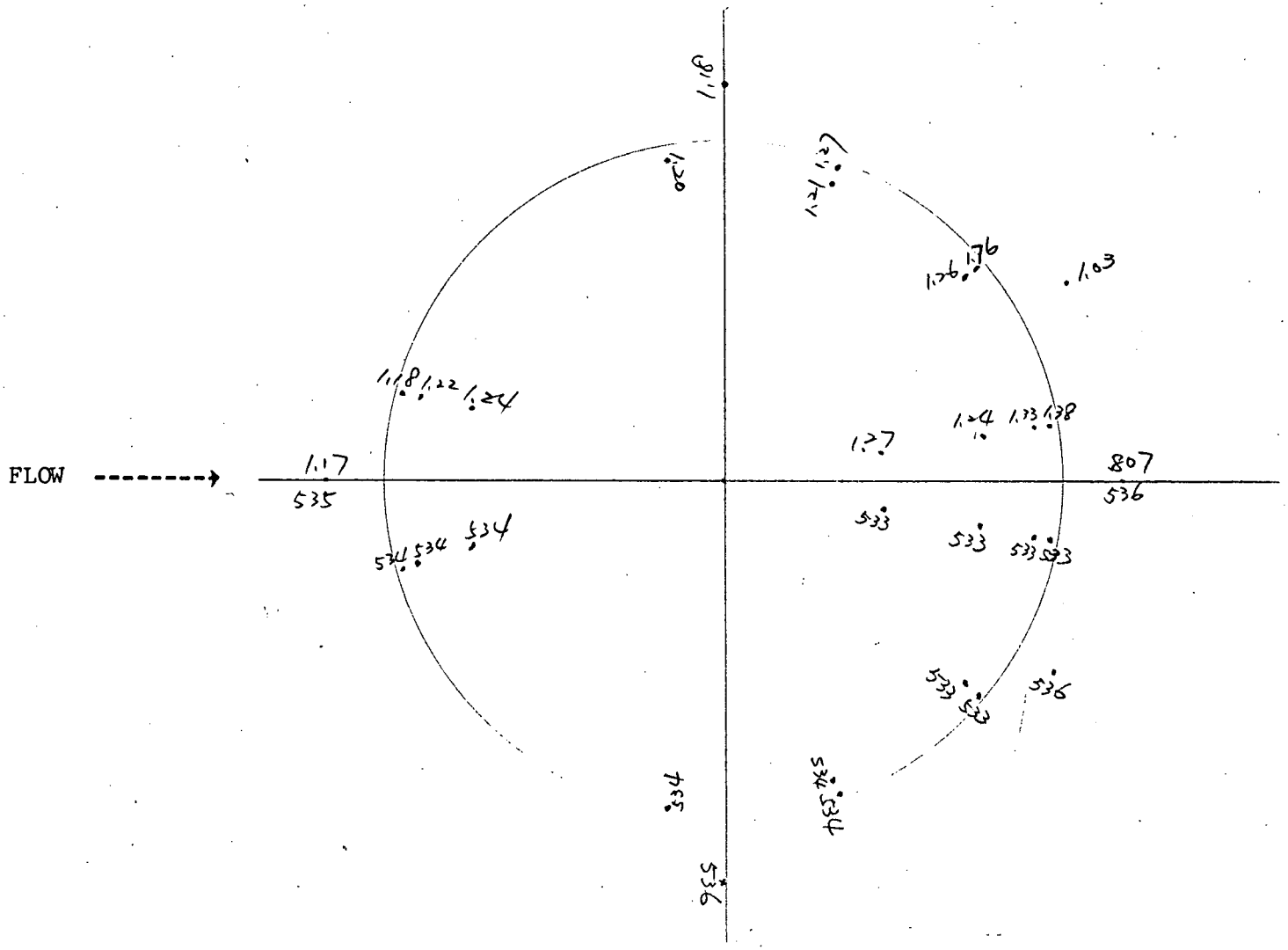

Fig. 12. PRESSURE (upper half, normalized by P-inf) AND TEMPERATURE (lower half, °R) DISTRIBUTIONS INSIDE AND AROUND THE EDGE OF CAVITY, UNDER CASE 1

FLOW ------->

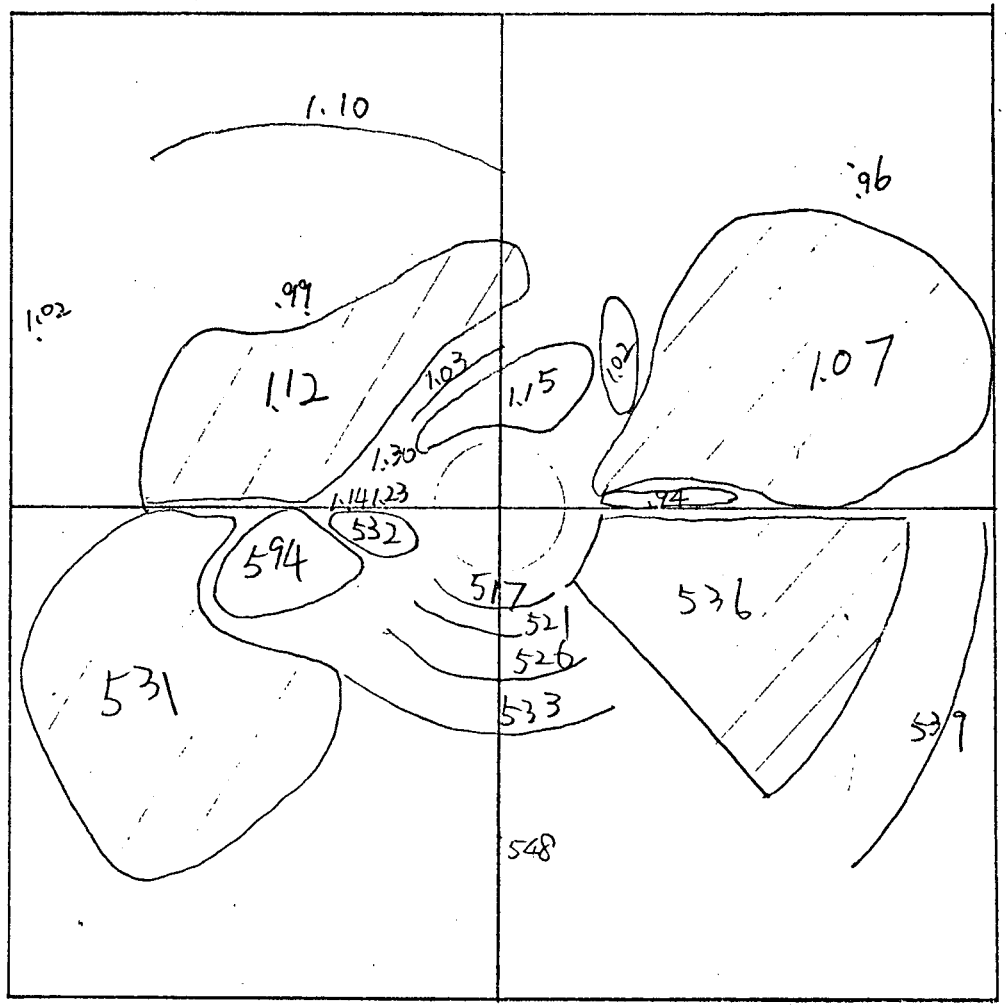

Fig. 13. ISOBAR (upper half, normalized by P-inf) AND ISOTHERM ^{o}R (lower half) UNDER CASE 2

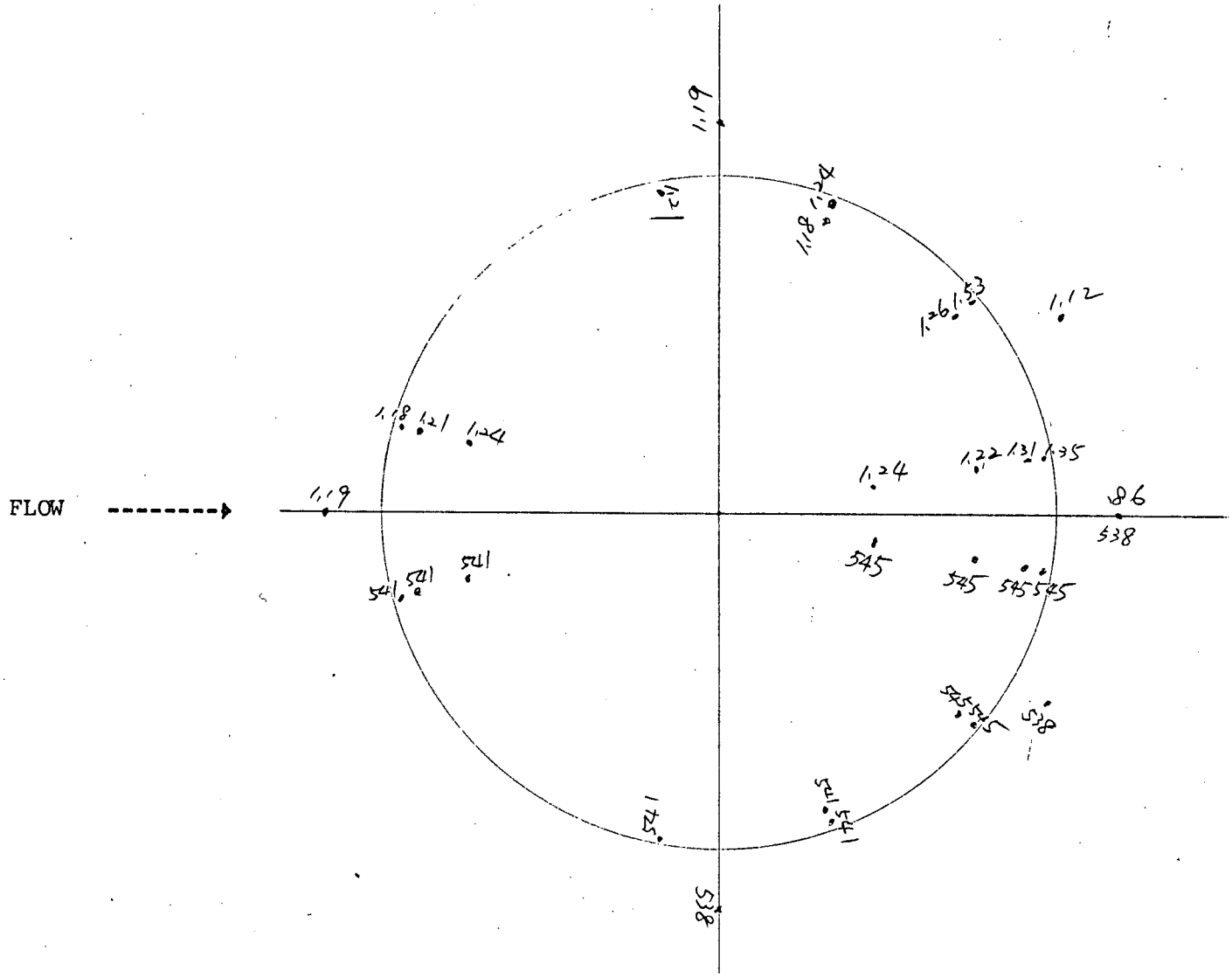

Fig. 14. PRESSURE (upper half, normalized by P-inf) AND TEMPERATURE (lower half, ^{o}R) DISTRIBUTIONS INSIDE AND AROUND THE EDGE OF CAVITY, UNDER CASE 2

FLOW ---------→

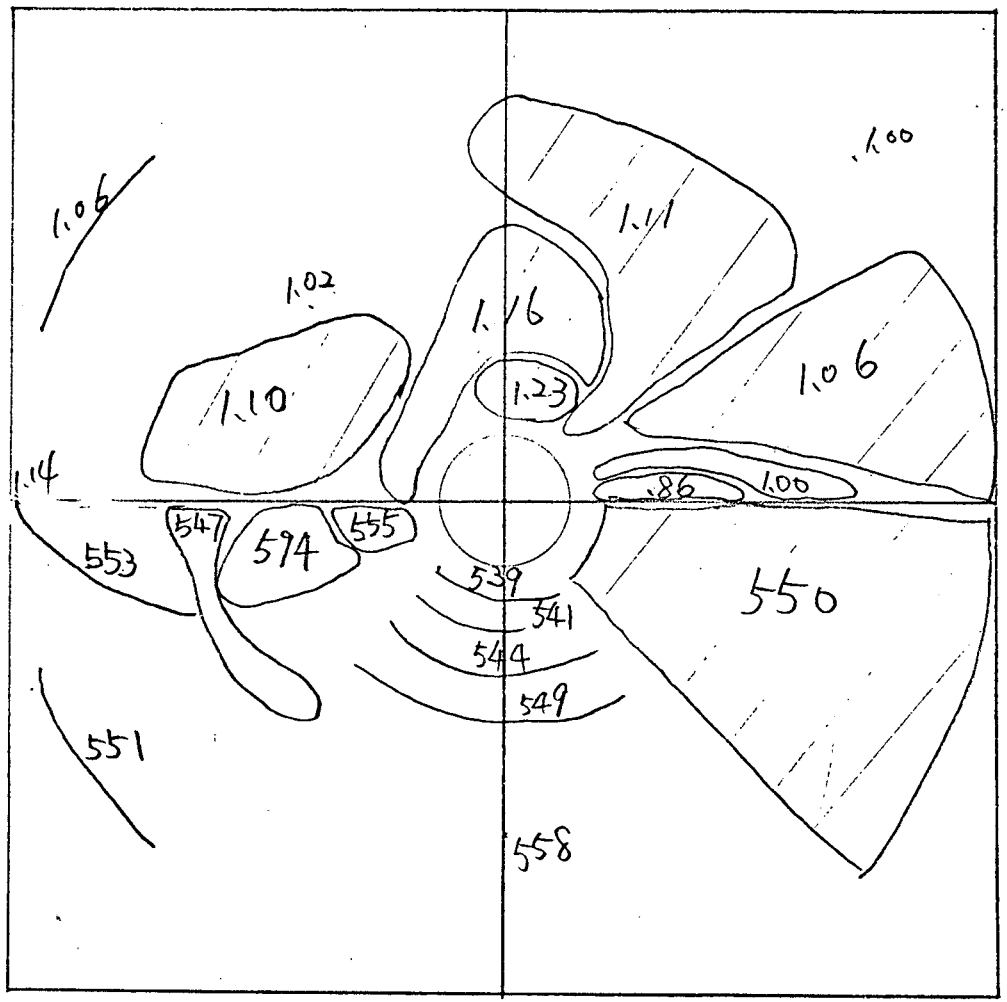

Fig. 15. ISOBAR (upper half, normalized by P-inf) AND
ISOTHERM °R (lower half) UNDER CASE 3

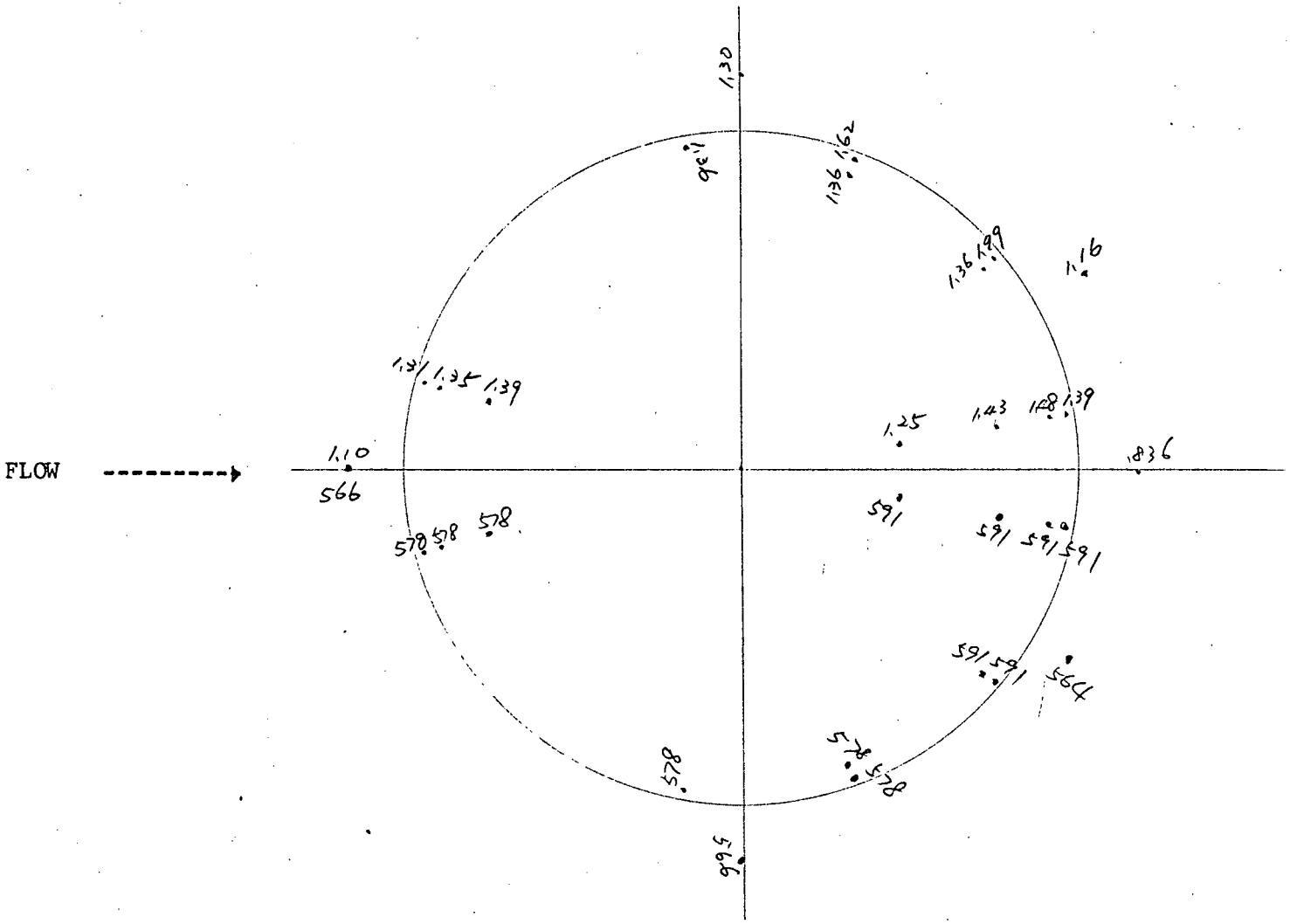

Fig. 16. PRESSURE (upper half, normalized by P-inf) AND TEMPERATURE (lower half, °R) DISTRIBUTIONS INSIDE AND AROUND THE EDGE OF CAVITY, UNDER CASE 3

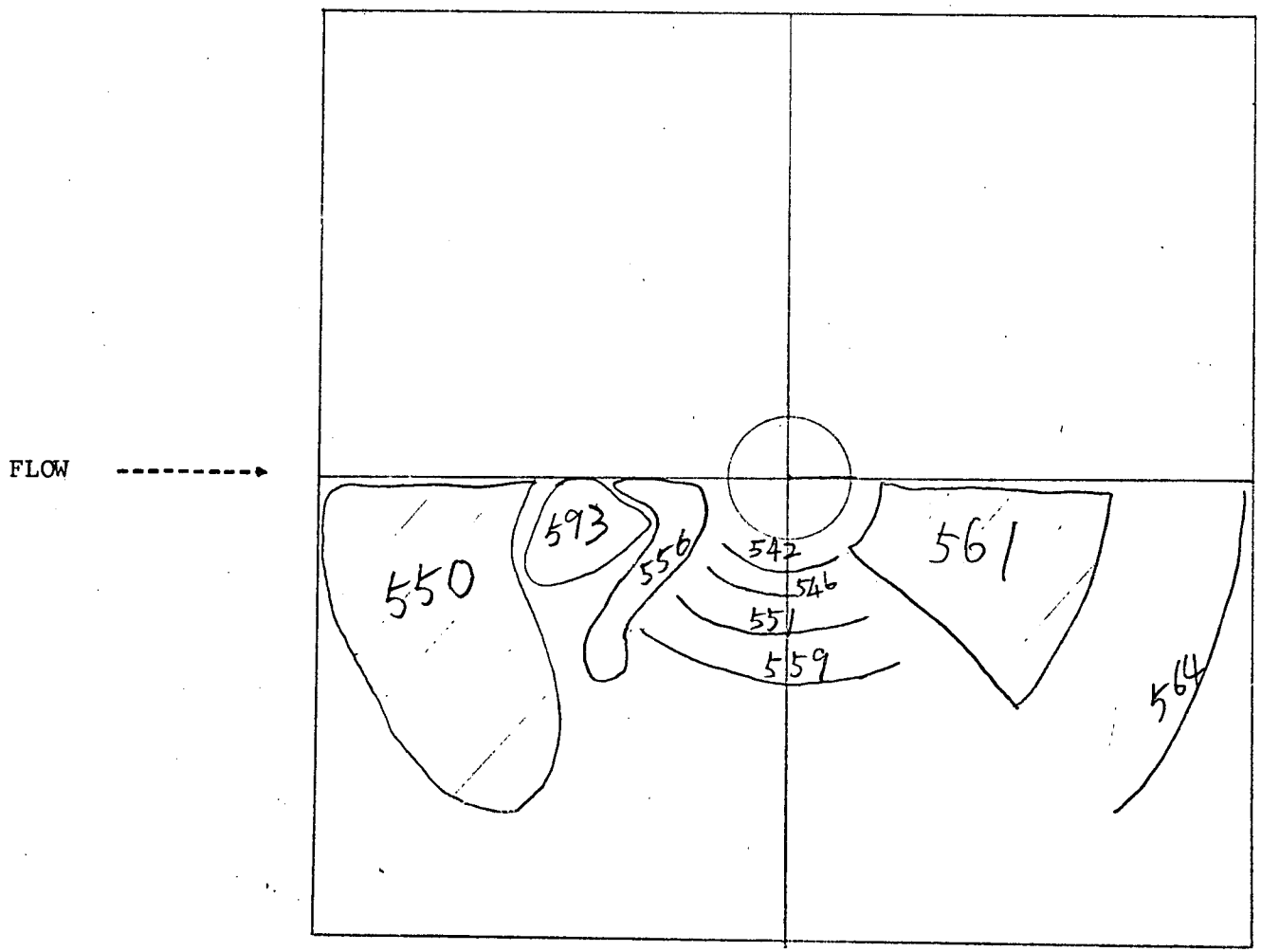

Fig. 17. ISOTHERMAL ZONES °R UNDER CASE 4

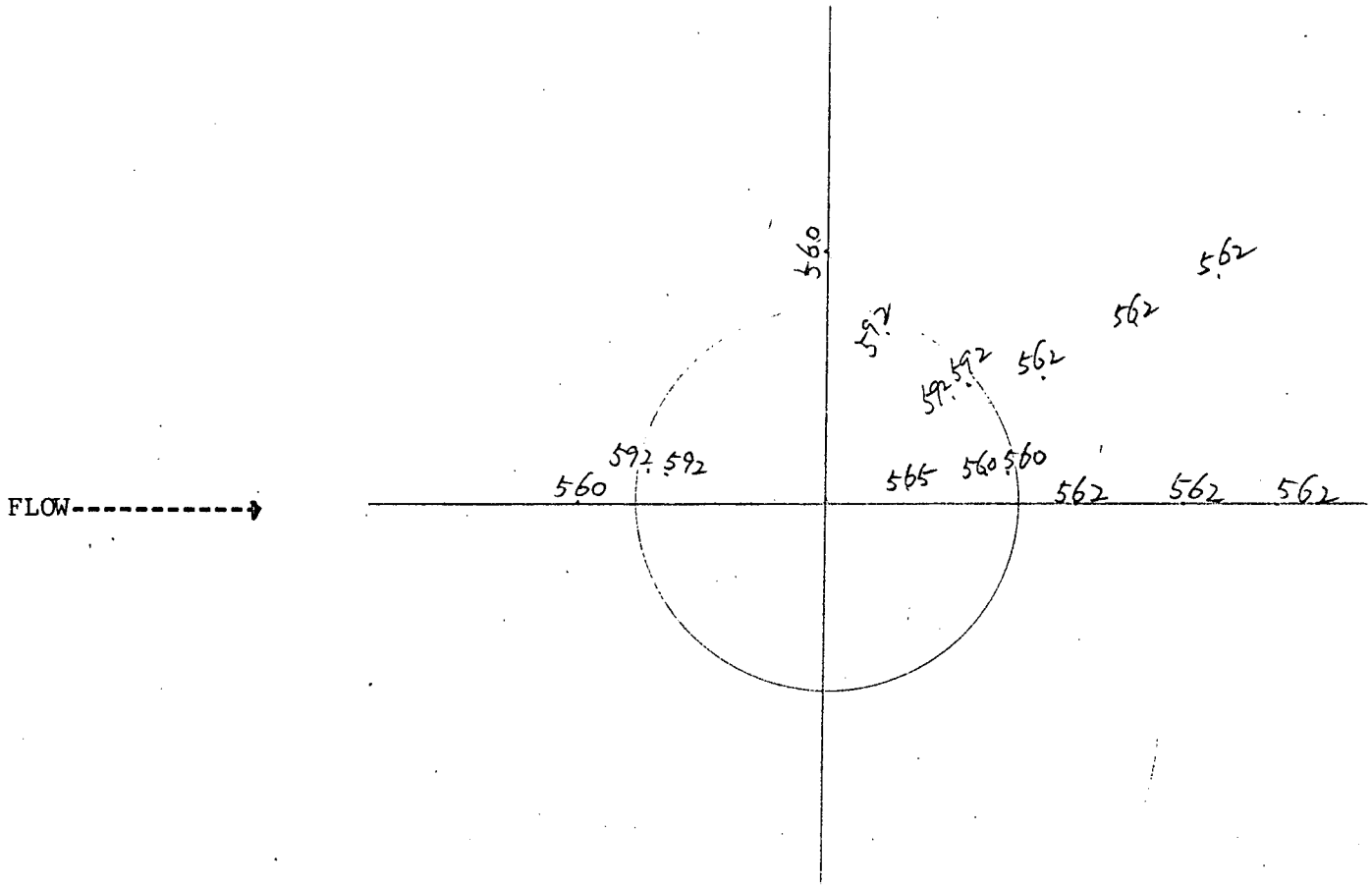

Fig. 18. TEMPERATURE DISTRIBUTION (°R) INSIDE AND AROUND THE EDGE OF THE CAVITY, UNDER CASE 4

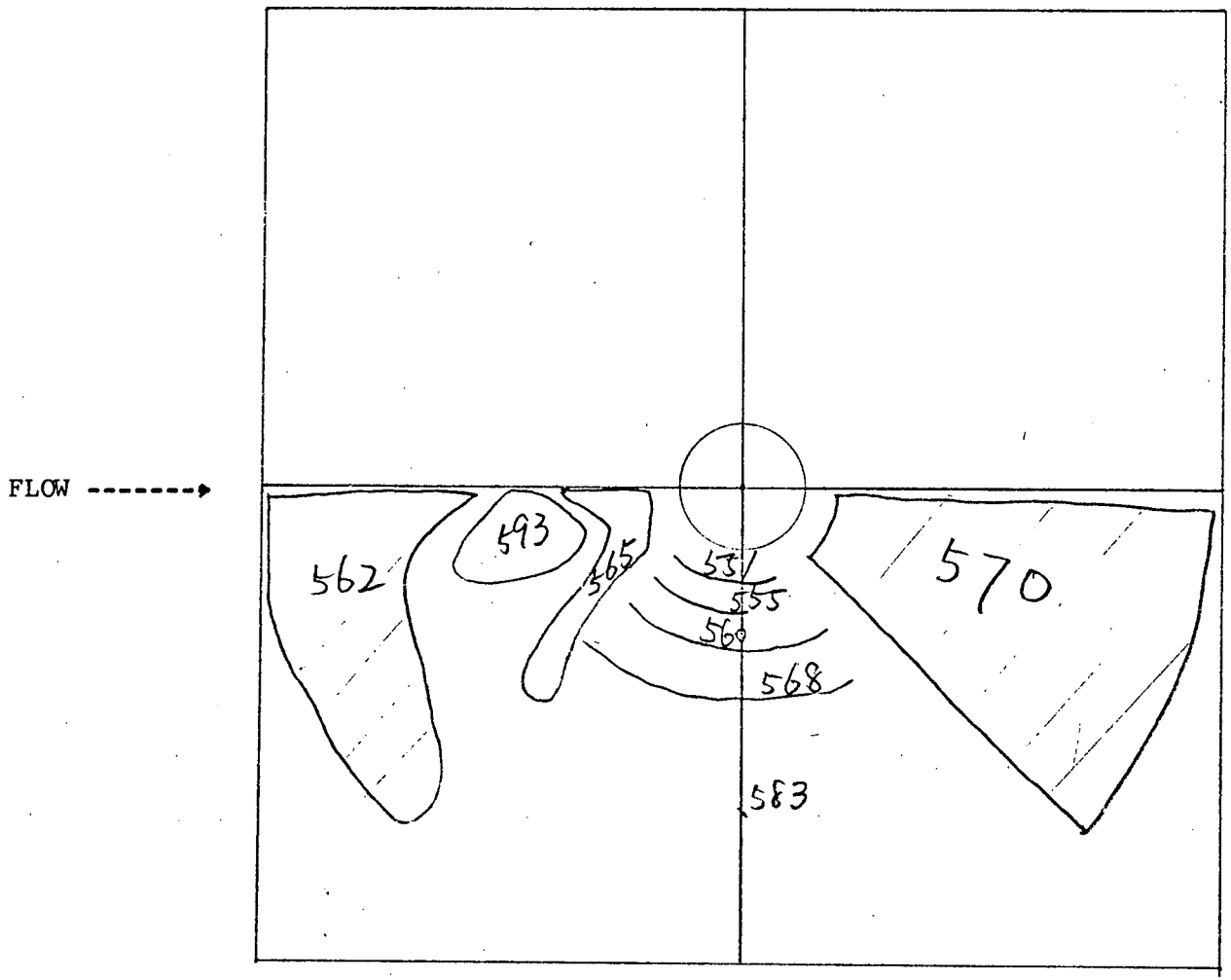

Fig. 19. ISOTHERMAL ZONES °R UNDER CASE 5

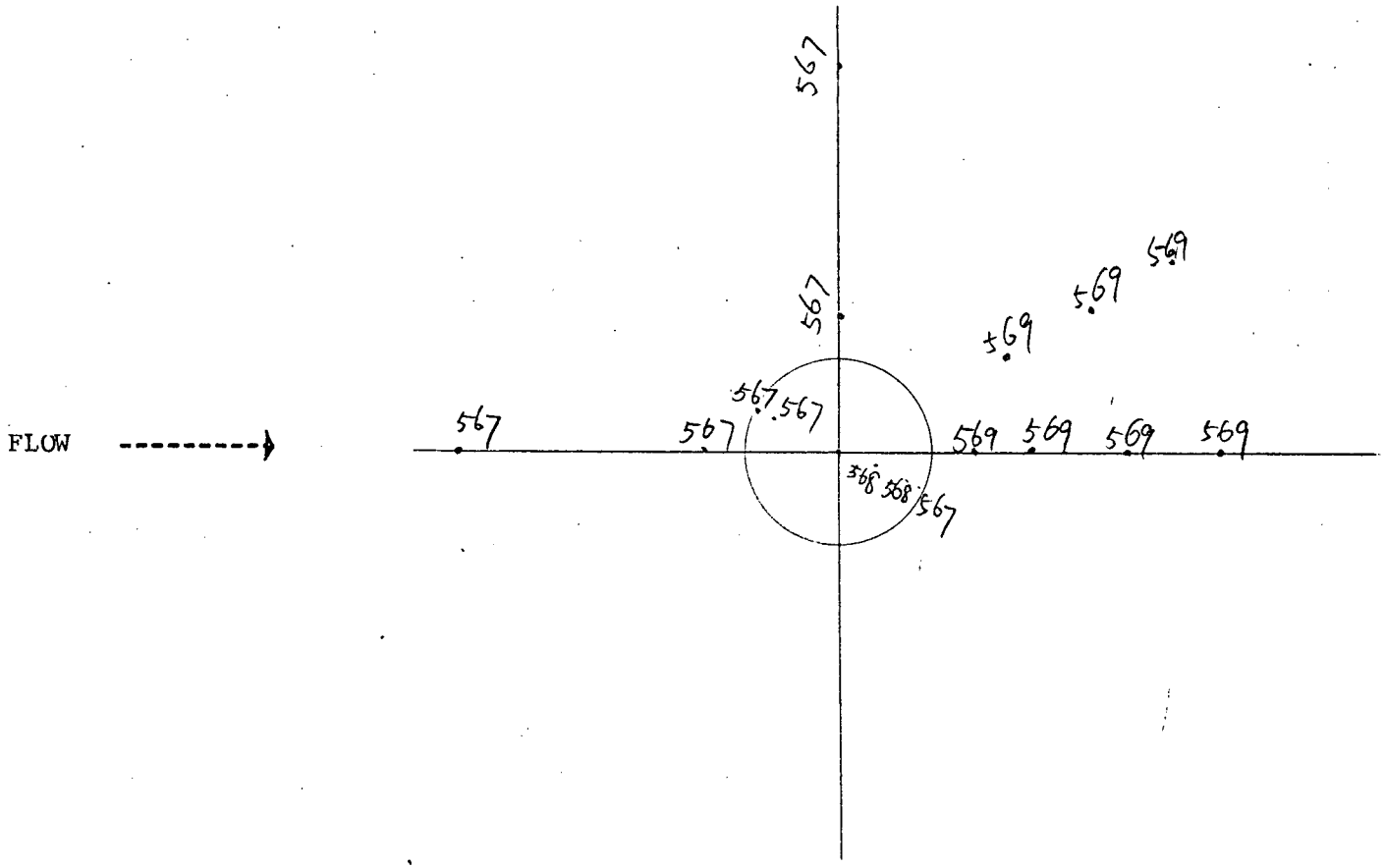

Fig. 20. TEMPERATURE DISTRIBUTION (°R) INSIDE AND AROUND THE EDGE OF THE CAVITY, UNDER CASE 5

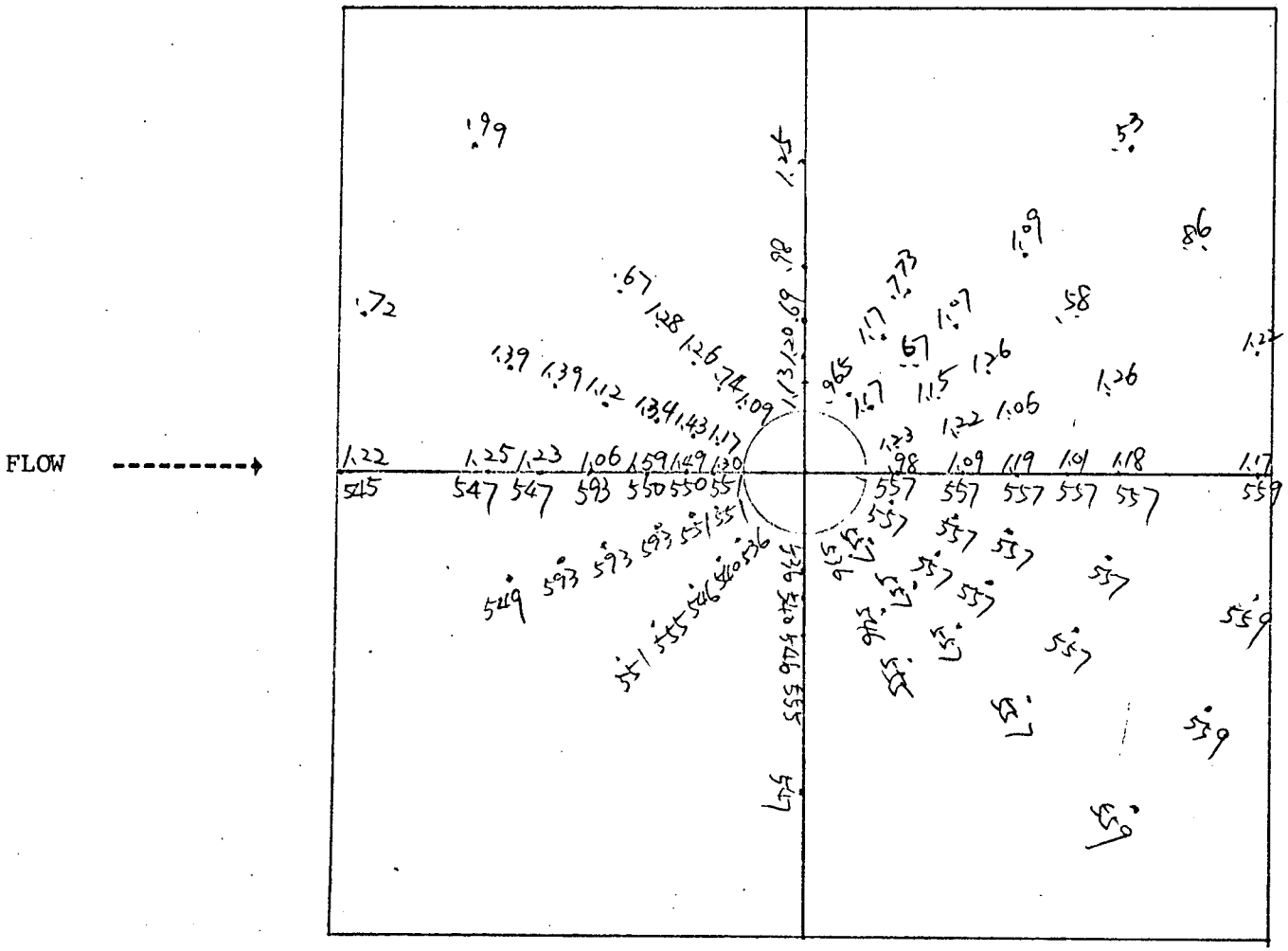

Fig. 21. PRESSURE DISTRIBUTION (upper half, normalized by P-inf) AND TEMPERATURE DISTRIBUTION °R (lower half) UNDER CASE 6

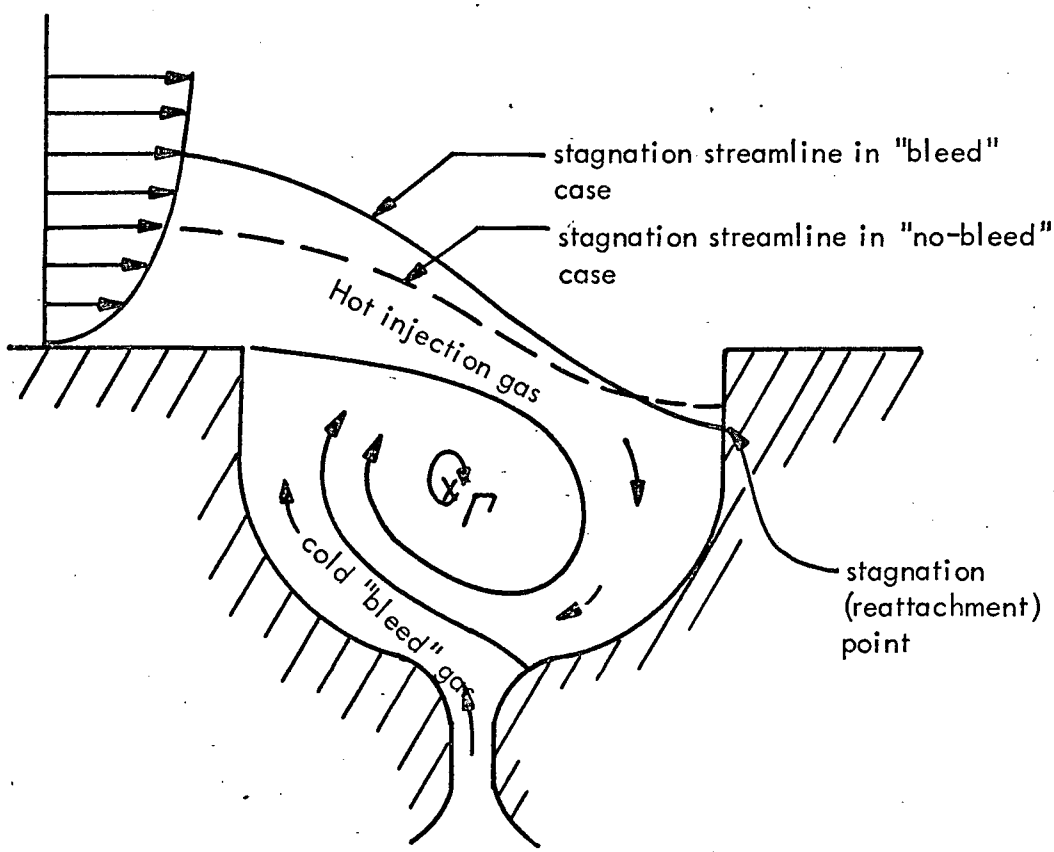

FIG. 22. Sketch of the Influence of Nozzle "Bleed" on the Flow in the Thrustor Cavity.

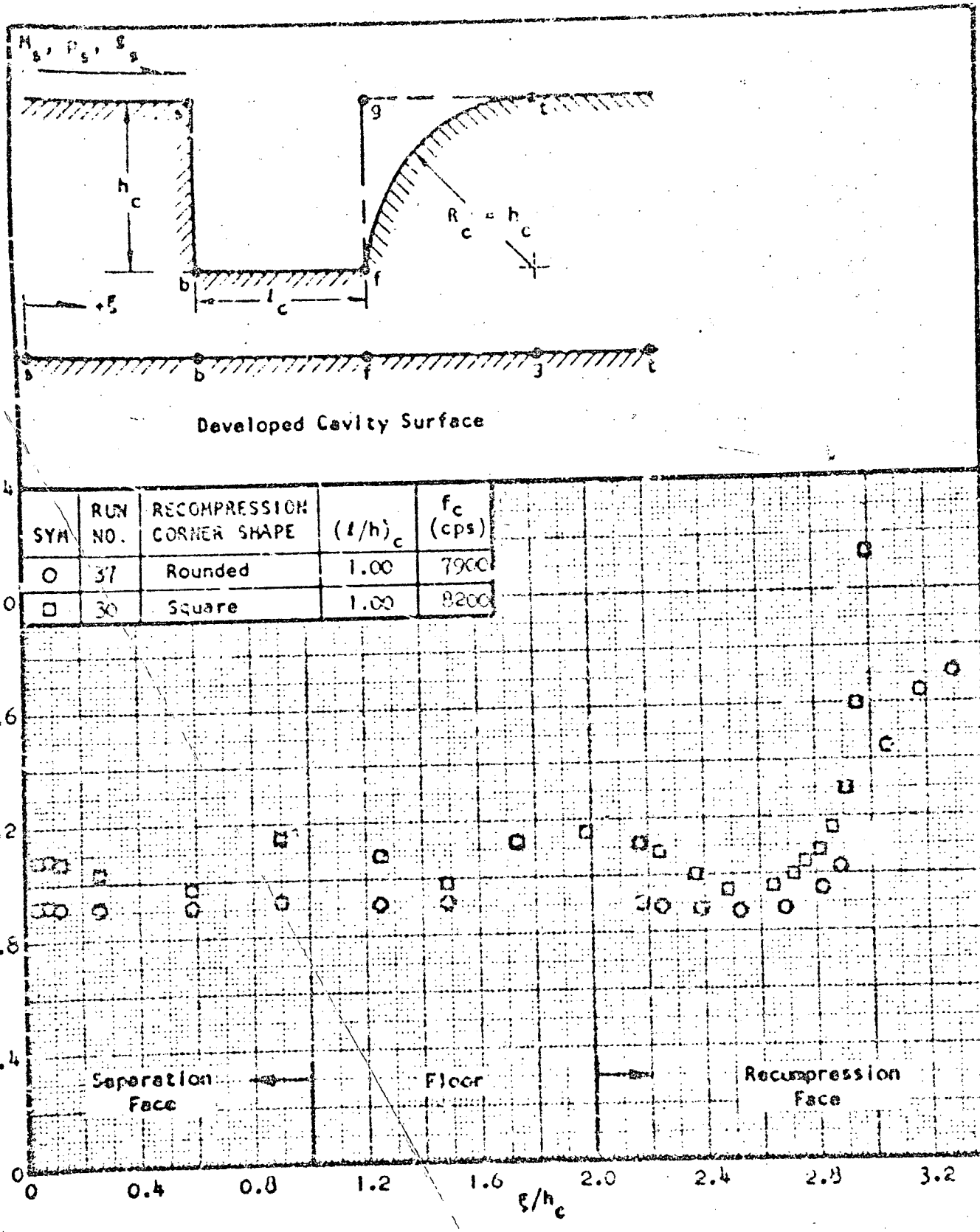

COMPARISON OF CAVITY WALL PRESSURE DISTRIBUTION OBTAINED FOR TWO RECOMPRESSION CORNER SHAPES. $M_s = 2.09$

TAKEN FROM REF.

FIGURE 23